Pramana – J. Phys. (2017) 88: 50
DOI 10.1007/s12043-016-1348-x

Effects of electron–phonon interaction and impurity on optical properties of hexagonal-shaped quantum wires

R KHORDAD[1,*] and H BAHRAMIYAN[2]

[1]Department of Physics, College of Sciences, Yasouj University, Yasouj, Iran
[2]Department of Optics and Laser Engineering, Marvdasht Branch, Islamic Azad University, Marvdasht, Iran
*Corresponding author. E-mail: rezakh2025@yahoo.com

MS received 7 December 2015; revised 1 June 2016; accepted 5 October 2016; published online 10 February 2017

Abstract. We have investigated the influence of electron–phonon (e–p) interaction and hydrogenic donor impurity simultaneously on energy difference, binding energy, the linear, nonlinear and total refractive index changes and absorption coefficients of a hexagonal-shaped quantum wire. For this goal, we have used finite-element method (FEM), a compact density matrix approach and an iterative procedure. It is deduced that energy difference and binding energy decrease by changing the impurity position with and without e–p interaction. The dipole matrix elements have complex behaviours in the presence of impurity with and without e–p interaction. The refractive index changes and absorption coefficients increase and shift towards lower energies by enhancing a_1 with central impurity. In the presence of central impurity, the absorption coefficients and refractive index changes enhance and shift toward higher energies when e–p interaction is considered.

Keywords. Quantum wire; optical properties; electronic properties.

PACS Nos 73; 73.21.−b

1. Introduction

Recently, with the rapid development of material production technology, the physical properties of low-dimensional semiconductor materials have aroused great interest. Among the low-dimensional structures, there has been a great deal of interest in the investigation of quantum wires. So far, many investigators studied the properties of quantum wires using several theoretical and experimental methods [1–8]. The study of quantum wires has been revolutionary in the fundamental sciences due to the potential applications of these structures in the technology of electronic and optoelectronics devices [9–11].

We know that Sakaki *et al* [12] proposed the concept of quantum wires for the first time in 1975. After this, with the advances in nanofabrication technologies, researchers could fabricate quantum wires of nanometre size with various cross-sections such as circular, V-shape, triangular, parallelogram, T-shape, and hexagonal shape [13–17]. For the past several years there has been a lot of interest in semiconductor quantum wires with complicated cross-sectional shapes, and considerable efforts have been devoted to study the physical properties of the wires. For example, Mohan *et al* [18] investigated the spectrum of luminescent hexagonal superlattice, formed by InP/InAs/InP nanotubes with the transversal cross-section of right hexagon shape. Vorobiev *et al* [19] studied the energy spectrum of an electron confined in the hexagonal-shaped quantum well. Makhanets *et al* [20] investigated the exciton spectrum in a multishell hexagonal semiconductor nanotube.

The physics of impurity states in semiconductors is very interesting because the physical properties of semiconductor devices are modified by hydrogenic impurities. The presence of Coulomb centre within the semiconductor nanostructures can have important effect on the physical properties of samples under study. After Bastard's pioneering work on the donor impurity in a semiconductor quantum well [21], many studies have been performed on impurity states in nanostructures [22–25].

The effects of impurity and the interaction between electrons and phonons on the physical properties of semiconductor nanostructures are interesting problems

in condensed matter physics. Low-dimensional semiconductor structures with and without impurity have been considered as potential candidates for new active electro-optical devices due to their unique properties resulting from the strength of the confinement potential. These structures show changed optical susceptibilities compared to those of the bulk semiconductors. As is known, among the optical properties, the study of refractive index changes, absorption coefficients, and third harmonic generations in nanostructures has been of great interest for researchers.

So far, many investigations have been done on the optical properties in quantum dots, quantum wells, and quantum wires under impurity effect and in the presence of electron–phonon interaction. For example, Maikhuri *et al* [26] have investigated the dependence of the linear and nonlinear intraband optical properties of ZnO quantum dots embedded in SiO_2 matrix. Recently, we have studied the optical absorption coefficients and refractive index changes in spherical quantum antidots with hydrogenic donor impurity at the centre [27]. Third harmonic generation in InAs/GaAs self-assembled quantum wires was studied by Sauvage *et al* [28]. Guo and Chen [29] presented the polaron effects on second-harmonic generation in quantum well within an electric field. Wang [30] calculated third harmonic generation in cylindrical parabolic quantum wires under an applied electric field.

To our knowledge, the effects of hydrogenic impurities and electron–phonon interaction on optical properties of a hexagonal-shaped quantum wire have not been investigated so far due to its particular shape (see figure 1). Therefore, the purpose of this article is to investigate the optical absorption coefficients and refractive index changes of a hexagonal-shaped ($GaAs/Ga_{0.5}In_{0.5}As$) quantum wire with and without impurity in the presence of electron–phonon interaction by using the finite-element method (FEM). We have used $GaAs/Ga_{0.5}In_{0.5}As$ because its parameters are known.

2. Theory and model

In the effective mass approximation, the Hamiltonian of an electron which interacts with bulk light phonons in the presence of hydrogenic donor impurity located at position $\mathbf{r}_0$ in a hexagonal core shell quantum wire is given by (see figure 1):

$$H = H_{\mathrm{e}} + H_{\mathrm{e-p}} - \frac{e^2}{\varepsilon|\mathbf{r} - \mathbf{r}_0|}, \tag{1}$$

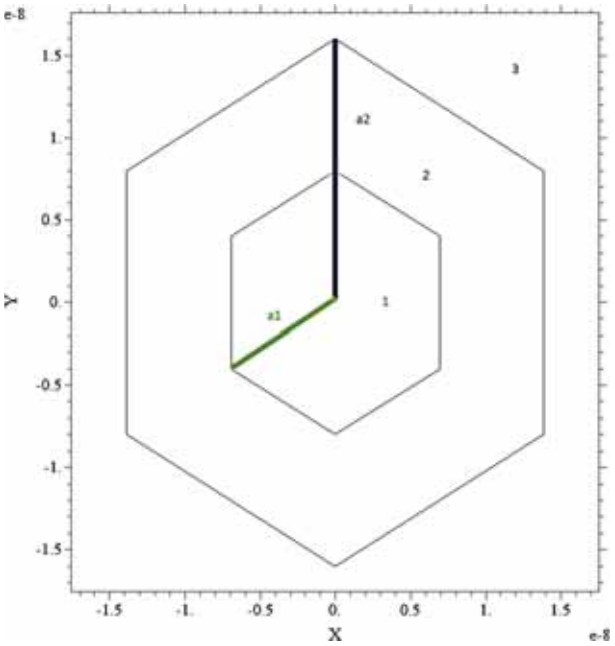

Figure 1. Geometric scheme of a hexagonal-shaped quantum wire.

with

$$H_{\mathrm{e}} = -\frac{\hbar^2}{2m^*}\nabla^2 + V(x, y). \tag{2}$$

Here m^* is the effective mass of the electron and the confining potential $V(x, y)$ is given by (see figure 1):

$$V(x, y) = \begin{cases} 0 & \text{region 1 } (0 < r < a_1) \\ V_0 & \text{region 2 } (a_1 < r < a_2), \\ \infty & \text{region 3 } (r \geq a_2) \end{cases} \tag{3}$$

where V_0 is the band offset between the conduction bands of semiconductors '1' and '2'.

The second term representing the optical phonon Hamiltonian is given by

$$H_{\mathrm{e-p}} = \sigma_{\mathrm{e}} \sum_{\mathbf{q}} \sqrt{\frac{\hbar q}{2\rho V c_l}} (b_{\mathbf{q},l} + b^{+}_{-\mathbf{q},l}) \mathrm{e}^{i\mathbf{q}\cdot\mathbf{R}}. \tag{4}$$

Here $b_{\mathbf{q},l}$ ($b^{+}_{-\mathbf{q},l}$) are the annihilation (creation) phonon operators, ρ is the material density, σ_{e} is the deformation potential, V is the volume of the crystal, c_l is the sound velocity, and $\mathbf{q} = (q_x, q_y, q_z)$ are the three-dimensional phonon wave vectors.

The last term in eq. (1) stands for the Coulomb interaction between the electron and the hydrogenic donor impurity. It is fully known that the calculation of energy levels and wave functions of a hexagonal core–shell quantum wire, analytically, is a nontrivial task.

Therefore, we intend to numerically find energy levels and wave functions of the Hamiltonian of eq. (1) with and without impurity, because these are required to calculate the optical properties.

In this work, we intend to employ the FEM to obtain wave functions and energy levels of the system numerically. The FEM is a numerical procedure for finding approximate solutions of differential equations [31]. FEM includes the use of mesh generation techniques for dividing a complex problem into small elements. The complex problem is usually a physical system with the underlying physics such as the Schrödinger equation, Poisson equation, or the Navier–Stokes equations expressed in the form of partial differential equation (PDF). It can be said that FEM is a powerful technique for numerically solving the partial differential equations.

We consider a volume of some material with known physical properties. The volume represents the domain of a boundary value problem to be solved. We construct a grid in real space using a discrete number of points. The eigenenergies and eigenstates of the electrons confined in a quantum wire are evaluated by solving the three-dimensional Schrödinger equation

$$-\frac{\hbar^2}{2m^*}\left(\frac{\partial^2}{\partial x^2}+\frac{\partial^2}{\partial y^2}+\frac{\partial^2}{\partial z^2}\right)\phi(x,y,z) + V(x,y,z)\,\phi(x,y,z) = E\phi(x,y,z), \tag{5}$$

where f and E are the wave function and energy levels. Also, $V(x,y,z) = V^{\text{conf}} + V^{\text{int}}$ where V^{conf} is the confining potential and $V^{\text{int}}(x,y,z) = -e^2/(\varepsilon|\mathbf{r}-\mathbf{r}_0|)$.

The operator ∇^2 is properly discretized by applying the standard three-point finite-difference approximation. In order to perform simulation numerically, one needs to discretize two-dimensional Schrödinger equation. The spatial derivative is approximated for all discretized space except on boundaries and is given by

$$\begin{aligned}\left[\frac{\partial^2}{\partial x^2}+\frac{\partial^2}{\partial y^2}+V(x,y)+V^{\text{int}}(x,y)\right]\phi^{(\text{int,out})}(x,y)\\ \approx \frac{1}{\Delta x^2}[\phi^{(\text{int,out})}(i+1,j)\\ -2\phi^{(\text{int,out})}(i,j)+\phi^{(\text{int,out})}(i-1,j)]\\ +\frac{1}{\Delta y^2}[\phi^{(\text{int,out})}(i,j+1)-2\phi^{(\text{int,out})}(i,j)\\ +\phi^{(\text{int,out})}(i,j-1)]\\ +[V(i,j)+V^{\text{int}}(i,j)]\phi^{(\text{int,out})}(i,j).\end{aligned} \tag{6}$$

The notation $\phi^{(\text{int,out})}(i,j)$ is used as $\phi^{(\text{int,out})}(i\Delta x, j\Delta y)$ where Δx and Δy are spatial spacings. Also, the superscripts 'int' and 'out' represent the wave function inside and outside the quantum wire. The continuity of the wave function on the quantum wire boundary is expressed by

$$\phi^{\text{int}}(x,y)|_{\text{in the boundary}} = \phi^{\text{out}}(x,y)|_{\text{in the boundary}}. \tag{7}$$

Also, the derivative of the wave function on the quantum wire boundary is given by

$$\frac{1}{m_1^*}\hat{n}\cdot\vec{\nabla}\phi^{\text{int}}|_{\text{in the boundary}} = \frac{1}{m_2^*}\hat{n}\cdot\vec{\nabla}\phi^{\text{out}}|_{\text{in the boundary}}. \tag{8}$$

Using eqs (6)–(8), the eigenvalue problem can be rewritten as

$$\begin{bmatrix}A_{11} & A_{12}\\ A_{21} & A_{22}\end{bmatrix}\begin{bmatrix}\phi^{\text{int}}\\ \phi^{\text{out}}\end{bmatrix} = E\begin{bmatrix}\phi^{\text{int}}\\ \phi^{\text{out}}\end{bmatrix}. \tag{9}$$

The eigenvalues and eigenfunctions of the system can be obtained by the diagonalization of eq. (9). After obtaining the eigenfunctions numerically, we have employed the perturbation theory. The wave function of the system can be calculated from the unperturbed wave functions as

$$|\Psi_i\rangle = |\phi_i\rangle + \sum_{i\neq j}\frac{\langle\phi_i|H_{\text{e-p}}|\phi_j\rangle}{E_i-E_j}|\phi_i\rangle. \tag{10}$$

3. Optical absorption coefficients and refractive index changes

In order to calculate the optical properties of our system, we first consider the interaction of a polarized monochromatic electromagnetic field with the system. Then, we use the density matrix formalism for computing the absorption coefficients and refractive index changes related to an optical transition.

The electromagnetic field vector with frequency ω can be expressed by

$$E(t) = Ee^{i\omega t} + E^*e^{-i\omega t}. \tag{11}$$

With respect to the time-dependent interaction of electromagnetic field with the system, the time evolution of the matrix elements of the one-electron density operator, ρ, is given by the von-Neumann equation [32–34]

$$\frac{\partial\rho_{ij}}{\partial t} = \frac{1}{i\hbar}[H_0 - erE(t),\rho]_{ij} - \Gamma_{ij}(\rho-\rho^{(0)})_{ij}, \tag{12}$$

where $\rho^{(0)}$ is the unperturbed density matrix, H_0 is the Hamiltonian of this system without the electromagnetic field $E(t)$, and q is the electronic charge.

The symbol [,] is the quantum mechanical commutator, Γ is the phenomenological operator responsible for damping due to collisions among electrons, etc. We can solve eq. (12) by applying the standard iterative method [35]. After obtaining the density matrix, we can determine the electronic polarization $P(t)$ and susceptibility $\chi(t)$ as

$$P(t) = \varepsilon_0\chi_\omega^{(1)}\tilde{E}e^{i\omega t} + \varepsilon_0\chi_{2\omega}^{(2)}\tilde{E}^2e^{2i\omega t} + \varepsilon_0\chi_0^{(2)}\tilde{E}^2 + \varepsilon_0\chi_{3\omega}^{(3)}\tilde{E}^3e^{3i\omega t} + \text{cc}, \quad (13)$$

where $\chi_\omega^{(1)}$, $\chi_{2\omega}^{(2)}$, $\chi_0^{(2)}$, and $\chi_{3\omega}^{(3)}$ are the linear susceptibility, second-harmonic generation, optical rectification, and third-harmonic generation, respectively. The electronic polarization of the nth order electronic polarization is as follows:

$$P^{(n)}(t) = \frac{1}{V}\text{Tr}(\rho^{(n)}qr), \quad (14)$$

where V and ρ are the volume of the system and the one-electron density matrix. Also ε_0 is the permittivity of free space, and the symbol Tr (trace) denotes the summation over the diagonal elements of the matrix.

In this paper, we have used the linear and the third-order nonlinear refractive index changes which are expressed as [36]

$$\frac{\Delta n^{(1)}(\omega)}{n_r} = \frac{\sigma_v^2e^2|M_{21}|^2}{2n_r^2\varepsilon_0} \times\left[\frac{E_{21}-\hbar\omega}{(E_{21}-\hbar\omega)^2+(\hbar\Gamma_{12})^2}\right], \quad (15)$$

$$\frac{\Delta n^{(3)}(\omega)}{n_r} = -\frac{\sigma_v e^4|M_{21}|^2}{4n_r^3\varepsilon_0}\frac{\mu cI}{[(E_{21}-\hbar\omega)^2+(\hbar\Gamma_{12})^2]^2} \times\left[4(E_{21}-\hbar\omega)|M_{21}|^2-\frac{(M_{22}-M_{11})^2}{(E_{21})^2+(\hbar\Gamma_{12})^2} \times\{(E_{21}-\hbar\omega)[E_{21}(E_{21}-\hbar\omega)-(\hbar\Gamma_{12})^2] -(\hbar\Gamma_{12})^2(2E_{21}-\hbar\omega)\}\right], \quad (16)$$

where σ_v is the carrier density, μ is the permeability, $E_{ij} = E_i - E_j$ is the energy difference, and $M_{ij} = |\langle i|x|j\rangle|$ is the electric dipole moment matrix element. Using eqs (15) and (16), one can write the total refractive index change as

$$\frac{\Delta n(\omega)}{n_r} = \frac{\Delta n^{(1)}(\omega)}{n_r} + \frac{\Delta n^{(3)}(\omega)}{n_r}. \quad (17)$$

The absorption coefficient $\alpha(\omega)$ is also calculated from the imaginary part of the susceptibility $\chi(\omega)$ as

$$\alpha(\omega) = \omega\sqrt{\frac{\mu}{\varepsilon_R}}\text{Im}[\varepsilon_0\chi(\omega)]. \quad (18)$$

The linear and third-order nonlinear absorption coefficients can be written as [32]

$$\alpha^{(1)}(\omega) = \omega\sqrt{\frac{\mu}{\varepsilon_R}}\left[\frac{\sigma_v e^2\hbar\Gamma_{12}|M_{21}|^2}{(E_{21}-\hbar\omega)^2+(\hbar\Gamma_{12})^2}\right], \quad (19)$$

$$\alpha^{(3)}(\omega, I) = -\omega\sqrt{\frac{\mu}{\varepsilon_R}}\left(\frac{Ie^4}{2n_r\varepsilon_0 c}\right) \times\frac{\sigma_v\hbar\Gamma_{12}|M_{21}|^2}{[(E_{21}-\hbar\omega)^2+(\hbar\Gamma_{12})^2]^2} \times\left\{4|M_{21}|^2 -\frac{(M_{22}-M_{11})^2[3E_{21}^2-4E_{21}\hbar\omega+\hbar^2(\omega^2-\Gamma_{12}^2)]}{(E_{21})^2+(\hbar\Gamma_{12})^2}\right\}, \quad (20)$$

where c is the speed of light in free space and I is the optical intensity of the incident wave, and it is given by

$$I = 2\sqrt{\frac{\varepsilon_R}{\mu}}|E(\omega)|^2. \quad (21)$$

Using eqs (19) and (20), one can express the total absorption coefficient as

$$\alpha(\omega, I) = \alpha^{(1)}(\omega) + \alpha^{(3)}(\omega, I). \quad (22)$$

4. Results and discussion

In this section, the energy difference E_{21}, binding energy, dipole matrix elements, absorption coefficients, and refractive index changes of a hexagonal-shaped quantum wire ($GaAs/Ga_{0.5}In_{0.5}As$) have been presented. The calculations have been performed with and without impurity in the presence of electron–phonon (e–p) interaction for various sizes of inner a_1 and outer a_2 hexagons. Here, we have selected $a_2 = 2a_1$. The parameters used in this present work are [36]: $m^*_{GaAs} = 0.067m_0$, $m^*_{GaInAs} = 0.045m_0$, $V_0 = 0.35$ eV, and $\hbar\Gamma = 0.4$ meV.

The geometrical scheme of a hexagonal-shaped quantum wire with sizes a_1 and a_2 respectively for the inner and outer hexagons is shown in figure 1.

Figure 2 shows the energy difference E_{21} of a hexagonal-shaped quantum wire as a function of impurity position y_0 with and without e–p interaction for $a_1 = 8$ nm and $a_2 = 16$ nm. One can see from the figure that energy difference is decreased by increasing the impurity position until 6 nm and then it increases. It is observed that the energy difference with e–p interaction is higher than without e–p interaction. It is

obvious that the energy difference with e–p interaction is obtained by using second-order perturbation.

Figure 3 displays the binding energy of a hexagonal-shaped quantum wire as a function of impurity location y_0 with and without e–p interaction for $a_1 = 8$ nm and $a_2 = 16$ nm. The binding energy is decreased when y_0 is increased. This behaviour is due to the enhancement of the distance between the impurity location and the position of maximum probability density of electron. When the distance is increased, the electron becomes less bound to the impurity. The binding energy with e–p interaction is lower than without e–p effect.

In figures 4 and 5, we have presented the dipole matrix elements of a hexagonal-shaped quantum wire as a function of impurity location y_0 with and without e–p interaction for $a_1 = 8$ nm and $a_2 = 16$ nm. It is observed from the figure that the dipole matrix elements with e–p interaction are enhanced. It is fully known that in the calculation of the dipole matrix elements there are two wave functions. We know that the dipole matrix element corresponds to the overlap of the wave function. With e–p interaction, the overlap between two different wave functions is increased.

One can observe from the figure that the dipole matrix elements have complex behaviours. But, approximately, all of them have two minima around $y_0 = 2$ and 5 nm and a maximum around $y_0 = 3$ nm. These behaviours correspond to the position of maximum probability density of electron in different states.

Figures 6–8 show linear, nonlinear, and total refractive index changes of a hexagonal-shaped quantum

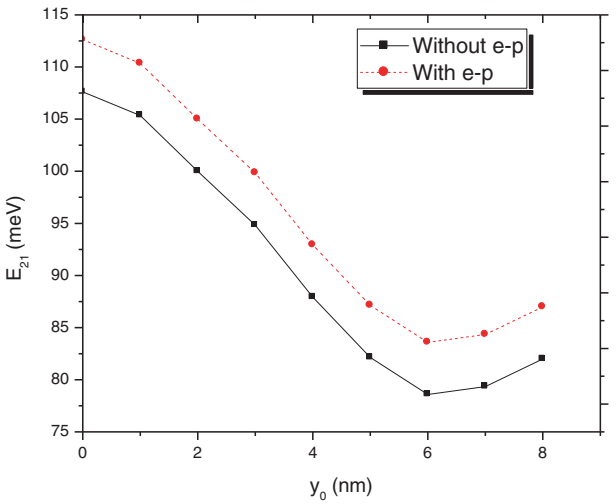

Figure 2. The energy difference E_{21} as a function of impurity position for $a_1 = 8$ nm and $a_2 = 16$ nm.

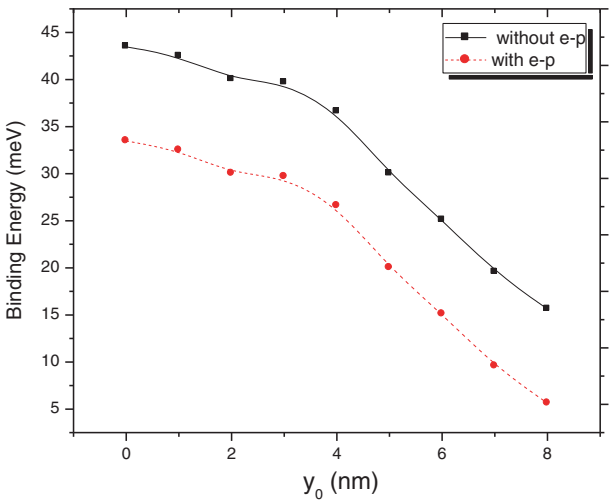

Figure 3. The binding energy vs. impurity position for $a_1 = 8$ nm and $a_2 = 16$ nm.

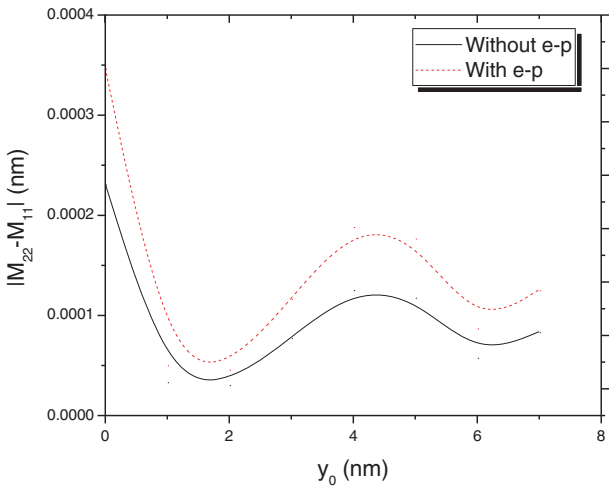

Figure 4. The dipole matrix elements ($M_{22} - M_{11}$) as a function of impurity position for $a_1 = 8$ nm and $a_2 = 16$ nm.

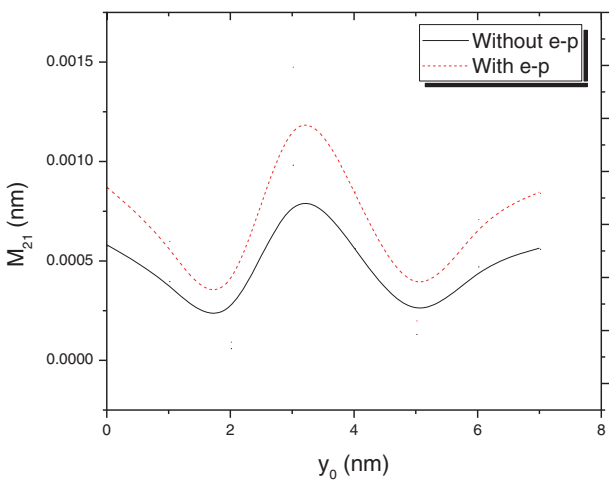

Figure 5. The dipole matrix element M_{21} as a function of impurity position for $a_1 = 8$ nm and $a_2 = 16$ nm.

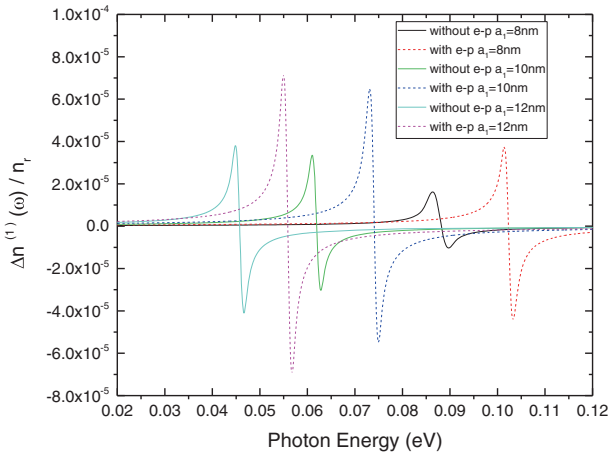

Figure 6. Linear refractive index changes vs. photon energy with and without e–p interaction for central impurity.

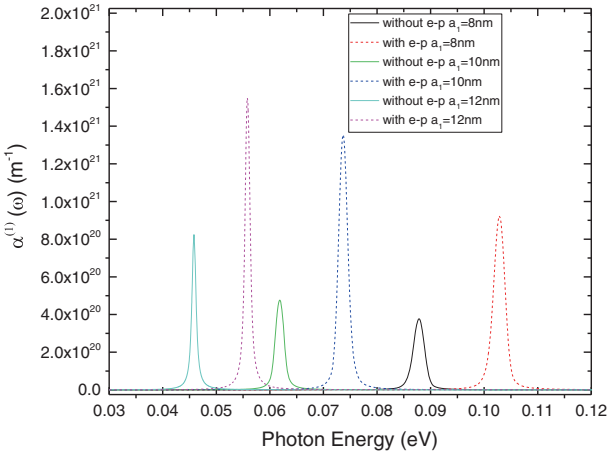

Figure 9. Linear absorption coefficients vs. photon energy with and without e–p interaction for central impurity.

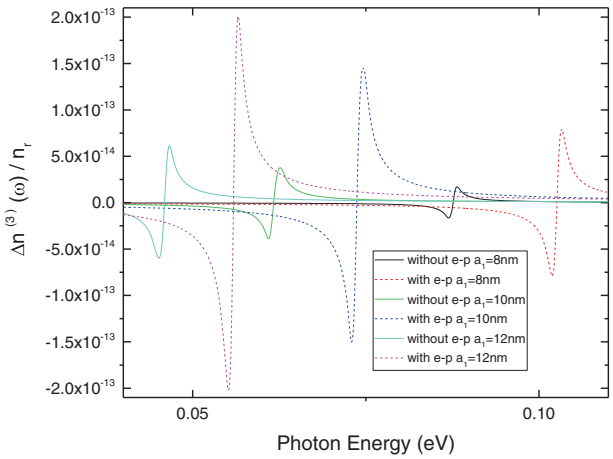

Figure 7. Nonlinear refractive index changes vs. photon energy with and without e–p interaction for central impurity.

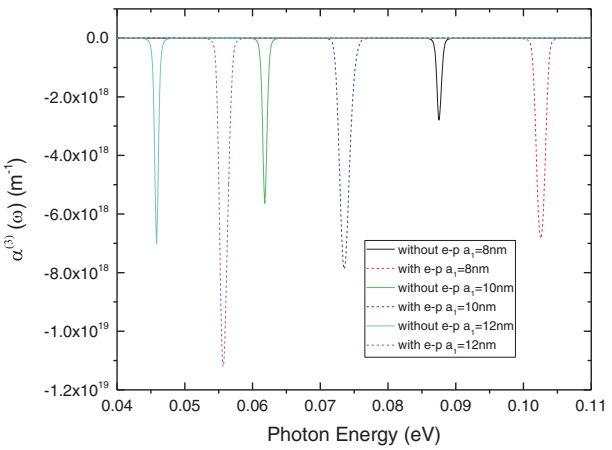

Figure 10. Nonlinear absorption coefficients vs. photon energy with and without e–p interaction for central impurity.

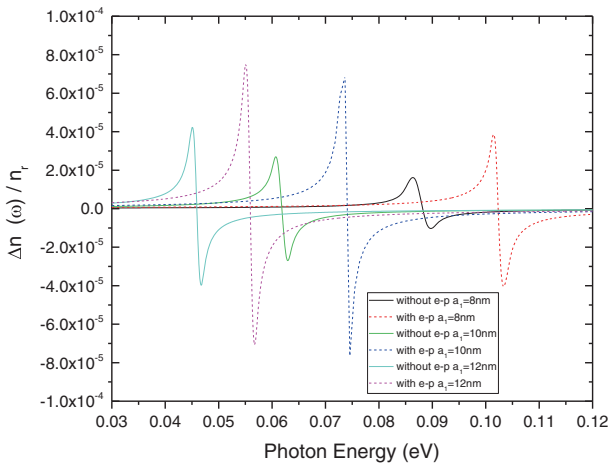

Figure 8. Total refractive index changes vs. photon energy with and without e–p interaction for central impurity.

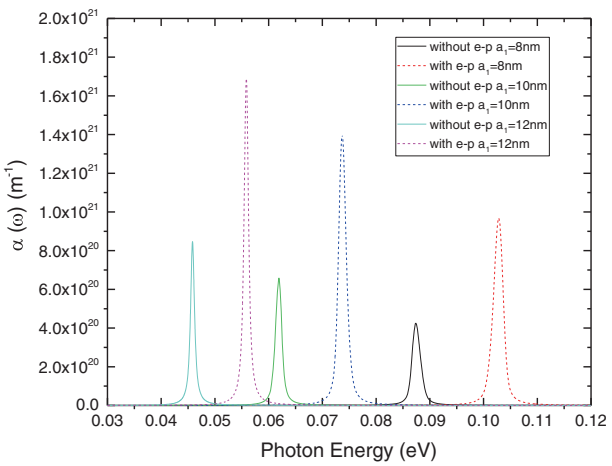

Figure 11. Total absorption coefficients vs. photon energy with and without e–p interaction for central impurity.

wire as a function of photon energy with and without e–p interaction for different values of a_1 with central impurity. In the figures, we have selected $a_2 = 2a_1$. It is seen from the figures that the refractive index changes enhance and shift towards higher energies by considering e–p interaction. As we see from the previous figures, the energy difference and dipole matrix elements increase by considering e–p interaction. Also, the refractive index changes increase and shift toward lower energies by increasing a_1. It is fully known that the quantum confinement and thereby the energy spacing is decreased by enhancing a_1. Therefore, the refractive index changes and absorption coefficients shift towards lower energies.

In figures 9–11, we have presented the linear, nonlinear, and total absorption coefficients of a hexagonal-shaped quantum wire as a function of photon energy for different values of a_1 with and without e–p interaction for central impurity. One can see from the figures that the absorption coefficients raise and shift towards lower energies by increasing a_1. It should be noted that the absorption coefficients enhance and shift towards higher energies by considering e–p interaction.

5. Conclusions

In this paper, we have presented the numerical results concerning the electronic and optical properties of a hexagonal-shaped quantum wire using FEM. In this regard, we have calculated energy difference, binding energy, refractive index changes, and absorption coefficients with and without e–p interaction in the presence of hydrogenic donor impurity. According to the results, it is found that the absorption coefficients and refractive index changes increase and shift towards lower energies by increasing a_1. But, the absorption coefficient and refractive index changes enhance and shift toward higher energies by considering e–p interaction. Also, the binding energy decreases by increasing the impurity positions. The dipole matrix elements have complex behaviours in the presence of impurity. In general, the sizes of inner a_1 and outer a_2 hexagons, impurity position, and e–p interaction have considerable effect on dipole matrix elements, energy difference and so the optical properties of a hexagonal-shaped quantum wire. It is worth mentioning that the results of this paper can be used to improve interpretations of the experimental data concerning the physical phenomena taking place in a subsurface level of the semiconductor materials with hexagonal-shaped structures.

References

[1] R Charguia, H Fenniche and R Bennaceur, *Physica E* **40**, 770 (2008)

[2] E Kasapoglu, F Ungan, C A Duque, U Yesilgul, M E Mora-Ramos, H Sari and I Sokmen, *Physica E* **61**, 107 (2014)

[3] V A Holovatsky, O M Voitsekhivsky and V I Gutsul, *Rom. J. Phys.* **53**, 833 (2008)

[4] T Sugaya, J P Bird, D K Ferry, A Sergeev, V Mitin, K Y Jang, M Ogura and Y Sugiyama, *Appl. Phys. Lett.* **81**, 727 (2002)

[5] B R Bulka, M Tolea and I V Dinu, *Phys. Rev. B* **74**, 205301 (2006)

[6] R Khordad and B Mirhosseini, *Pramana – J. Phys.* **85**, 723 (2015)

[7] S I Molina, T Ben, D L Sales, J Pizarro, P L Galindo, M Varela, S J Pennycook, D Fuster, Y Gonzalez and L Gonzalez, *Nanotechnol.* **17**, 5652 (2006)

[8] A L Vartanian, A L Asatryan and L A Vardanyan, *Physica E* **47**, 134 (2013)

[9] W Lei, Y H Chen, Y L Wang, X Q Huang, Ch Zhao, J Q Liu, B Xu, P Jin, Y P Zeng and Z G Wang, *J. Crystal Growth* **286**, 23 (2006)

[10] R Khordad and B Mirhosseini, *Opt. Spectrosc.* **117**, 434 (2014)

[11] N Arunachalam, A John Peter and C W Lee, *Physica E* **44**, 222 (2011)

[12] H Sakaki and T Sugana, *J. Jpn Soc. Appl. Phys.* **44**, 1131 (1975)

[13] G Rezaei, S M Azami and B Vaseghi, *Phys. Status Solidi B* **249**, 1459 (2012)

[14] R Khordad and H Bahramiyan, *J. Appl. Phys.* **115**, 124314 (2014)

[15] R Khordad, *Opt. Quant. Electron.* **46**, 283 (2014)

[16] C A Duque, M E Mora-Ramos, E Kasapoglu, F Ungan, U Yesilgul, S Sakiroglu, H Sari and I Sokmen, *J. Lumin.* **143**, 304 (2013)

[17] R Khordad and H Bahramiyan, *Mod. Phys. Lett. B* **29**, 1550078 (2015)

[18] P Mohan, J Motohisa and T Fukui, *Appl. Phys. Lett.* **88**, 133105 (2006)

[19] Yu V Vorobiev, V R Vieira, P P Horley, P N Gorley and J G Hernandez, *Sci. China Ser. E: Technol. Sci.* **52**, 15 (2009)

[20] O M Makhanets, V I Gutsul, N R Tsiupak and O M Voitsekhivska, *Condens. Matter Phys.* **15**, 33704 (2012)

[21] G Bastard, *Phys. Rev. B* **24**, 4714 (1981)

[22] R Khordad and H Bahramiyan, *Eur. Phys. J. Appl. Phys.* **67**, 20402 (2014)

[23] D S A Coden, R H Romero, A Ferrón and S S Gomez, *J. Phys. B: At. Mol. Opt. Phys.* **46**, 065501 (2013)

[24] E Yu Perlin, *Opt. Spectrosc.* **88**, 439 (2008)

[25] R Khordad and H Bahramiyan, *Physica E* **66**, 107 (2015)

[26] D Maikhuri, S P Purohit and K C Mathur, *AIP Adv.* **2**, 012160 (2012)

[27] S Davatolhagh, R Khordad and A R Jafari, *Semiconductors* **48**, 596 (2014)

[28] S Sauvage, P Boucaud, F Glotin, R Prazeres, J M Ortega, A Lemaitre, J M Gerard and V Thierrymieg, *Phys. Rev. B* **59**, 9830 (1999)
[29] K X Guo and C Y Chen, *J. Phys. Condens. Matter* **7**, 6583 (1995)
[30] G Wang, *Phys. Rev. B* **72**, 155329 (2005)
[31] D V Hutton, *Fundamentals of finite element analysis* (McGraw-Hill, New York, 2004)
[32] R W Boyd, *Nonlinear optics*, 2nd edn (Academic Press, 2003)
[33] D Ahn and S L Chuang, *IEEE J. Quant. Electron.* **23**, 2196 (1987)
[34] D E Aspnes, *Phys. Rev. B* **14**, 5331 (1976)
[35] K J Kuhn, G U Lyengar and J Yee, *J. Appl. Phys.* **70**, 5010 (1991)
[36] S Adachi, *J. Appl. Phys.* **58**, R1 (1985)